
Article:
Zhou, Y and Califano, M orcid.org/0000-0003-3199-3896 (2021) Decoupling Radiative and Auger Processes in Semiconductor Nanocrystals by Shape Engineering. The Journal of Physical Chemistry Letters, 12 (37). pp. 9155-9161. ISSN 1948-7185

https://doi.org/10.1021/acs.jpclett.1c02300

Decoupling Radiative and Auger Processes in Semiconductor Nanocrystals by Shape Engineering

Yang Zhou[†] and Marco Califano[*,†,‡]

† *Pollard Institute, School of Electronic and Electrical Engineering, University of Leeds, Leeds LS2 9JT, United Kingdom*

‡ *Bragg Centre for Materials Research University of Leeds, Leeds LS2 9JT, United Kingdom*

E-mail: m.califano@leeds.ac.uk

Abstract

One of the most challenging aspects of semiconductor nanotechnology is the presence of extremely efficient non-radiative decay pathways (known as Auger processes) that hinder any attempt at creating population inversion and obtaining gain in nanocrystals. What is even more frustrating is that, in most cases, the strategies adopted to slow down Auger in these nanostructures also lead to a comparable increase in the radiative recombination times, so that there is no overall improvement from the point of view of their applicability as emissive media. Here we present a comprehensive theoretical characterisation of CdTe tetrapods and show that in these versatile nanostructures it is possible to achieve a complete decoupling between radiative and Auger processes, where the latter can be strongly suppressed compared to spherical structures, by careful shape engineering, without affecting the efficiency of radiative recombination.

Graphical TOC Entry

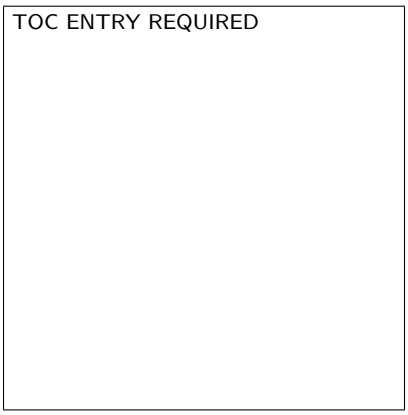

Keywords

Nanocrystals, tetrapods, CdTe, Auger processes, pseudopotential method

Semiconductor nanocrystals (NCs) have attracted widespread attention as light-emitting materials and have been utilized in fluorescent bio-labelling,[1] LEDs[2] and lasers,[3] thanks to their peculiar size-dependent optical and electronic properties.[4–6] Indeed, their emission can span the whole visible spectrum[7,8] achieving nearly unitary photoluminescence quantum yields.[9] Ironically, the same properties that make these systems attractive for lighting applications are also responsible for the efficiency of the non-radiative recombination mechanisms that plague them, which is commonly attributed to the suppression of momentum conservation and the enhancement of Coulomb interaction occurring in strongly confined systems.[10] In particular, in the presence of high doping concentrations or high excitation powers, Auger recombination (AR) effectively competes with radiative recombination, leading, among other effects, to fluorescence intermittency,[11] and limiting optical gain.[3] In this non-radiative process, the energy produced from the recombination of an electron-hole pair is transferred to a third carrier, either the electron or the hole, promoting it to an excited state. Another related process, Auger cooling (AC), is responsible for the extremely efficient electron thermalization observed in NCs, which occurs via an electron-hole scattering mechanism, where a hot electron relaxes to the ground state by transferring its excess energy to a hole in its ground state and exciting it to a deeper state, proving detrimental for applications in intraband infrared photodetection and hot-electron solar cells.[12–14]

Therefore, devising effective strategies to overcome such extremely efficient non-radiative processes, enabling the creation of population inversion and the attainment of the theoretically achievable optical gain in nanocrystals, is one of the priorities that has occupied the NC synthesis community for long time.

As the Auger rates depend on the coupling integral, that contains both initial and final states, i.e., the wave functions of both electron and hole, the approach most commonly used is based on the reduction of their overlap in real space.

This can be achieved through structure modification: (i) elongation - the synthesis of nanorods with large aspect ratios of length over radius has been shown to promote spatial separation of electron and hole wave functions, leading to a reduction in AR rates;[15] (ii) asymmetrical heterostructuring - dot-in-a-rod (dot@rod) structures, where the the spherical quantum dot is embedded in a rod-shaped shell made of a different material and is generally located close to one of the rod's extremities, achieve a localization of the hole in the core whereas the electron is delocalized throughout the rod, leading to a reduction in the AR rates;[16] (iii) symmetrical heterostructuring - the growth of a shell of a different semiconductor material, with a specific electronic structure, around the spherical nanocrystal core, can lead to a type II (or quasi type II) band alignment at the heterointerface, resulting in complete (or partial) spatial segregation of electron and hole, each confined to a different material,[17,18] markedly suppressing Auger processes.[19,20] However, the synthesis methods for some of these structures are complex (as it is the case for successive ion layer adsorption and reaction - SILAR), inevitably increasing both growth time and energy consumption[18,21] and consequently the processing cost.

In contrast to structure and size engineering, the modification of the conduction band states' wave function composition in reciprocal space, which leads to a decreased overlap with the holes' wave function *in k-space*, is another approach recently proposed to suppress Auger processes.[22] Unfortunately all of these methods, by reducing el-h overlap, also lead to an undesired suppression of radiative recombination,[23] making these systems well suited for solar energy harvesting applications (such as PV or photocatalysis), but not for applications as light emitters (LEDs and lasers). The close link existing between AR and radiative recombination (RR) is exemplified by the peculiar scaling $\tau_{AR} \propto V\tau_{RR}$ (where V is the NC volume), observed in CdTe/CdSe core/shell NCs.[19]

Devising strategies to suppress Auger processes, while retaining, at the same time, the high radiative rates and PL quantum yields that characterise these systems, is therefore crucial for the effective exploitation of their full potential as emissive media. Here we

show that this is indeed possible and can be achieved by structure manipulation, and, in particular, by combining elongation (i) with symmetrical growth (iii), in branched homostructures, also known as tetrapods (TPs).

Thanks to their easy fabrication and processability, and their versatile electronic and optical properties, tetrapod-shaped nanocrystals have recently attracted large interest.[24–26] In this family, CdTe TPs are the simplest structures in terms of synthesis and size control.[24] Their electronic structure, charge dynamics,[27] optical,[28] mechanical and electrical[29] properties have been investigated both experimentally and theoretically however, to the best of our knowledge, Auger processes have not been explicitly considered nor systematically studied.

In this paper we present a theoretical characterisation, based on the atomistic semiempirical pseudopotential method[30] (SEPM), of CdTe TPs covering a wide range of aspect ratios $0.8 \leq \rho \leq 6.7$ (including experimentally relevant ones[31–33]), of arm length (L) over arm diameter (D), for 1.75 nm $\leq L \leq$ 14 nm and 1.75 nm$\leq D \leq$ 3.5 nm, containing from about 1000 to over 6600 atoms. We recently used the same theoretical framework to design heterostructured, core/arms TPs for selective CO_2 reduction to CH_4.[34] In that work the main aims were to achieve (i) charge separation between core and arms (to ensure that the photogenerated electron and hole did not recombine before reaching the surface and reacting with CO_2 and H_2O), and (ii) an accurate conduction band minimum positioning between the reduction potentials of CO_2 to CH_4, and of H_2O to H_2 (to guarantee good selectivity). This was achieved using TPs with a CdTe core and CdSe arms, which resulted, *inter alia*, in orders of magnitude decrease in the radiative recombination rate with increasing arm length, as a consequence of the different localisation of the ground state electron and hole (the latter being localised in the core and the former in the arms), caused by the type II band alignment at the CdTe/CdSe interface.

The question we will address here is, instead, whether AC and AR can be suppressed efficiently *without* affecting radiative recombination, therefore achieving a complete de-

coupling between radiative and Auger processes.

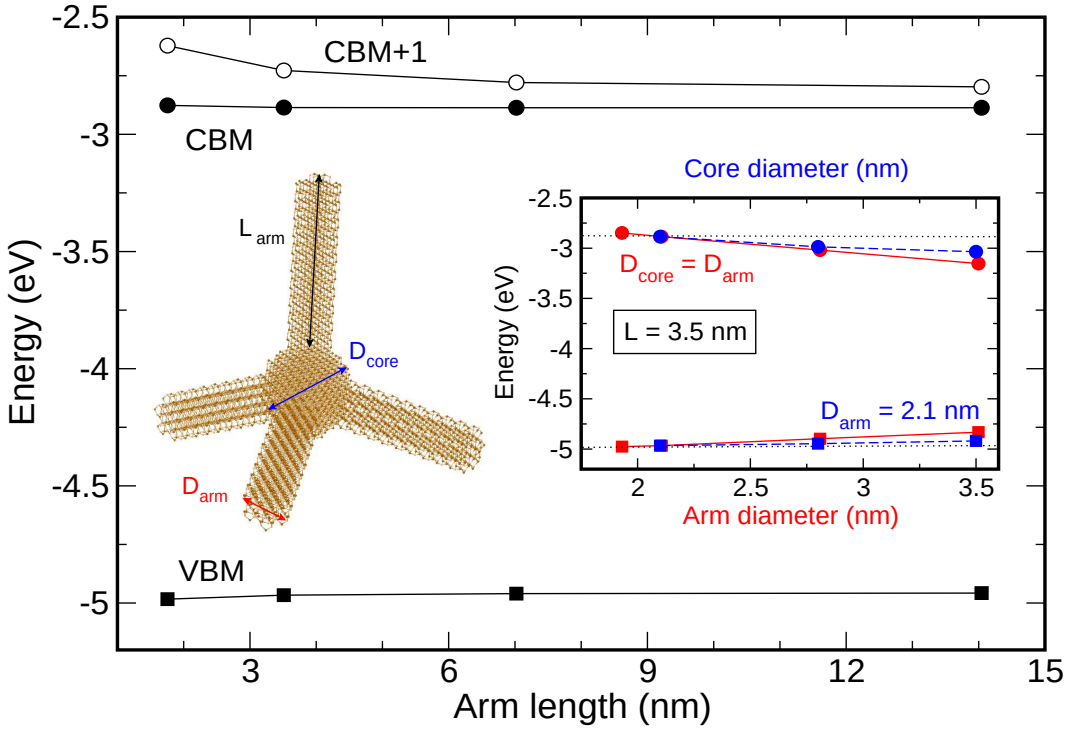

Figure 1: CdTe TP valence (squares) and conduction (circles) band edge energies, calculated, with respect to vacuum, as a function of: (mainframe) arm length L, for $D = 2.1$ nm; (inset) arm diameter D_{arm}, assuming the core diameter $D_{\text{core}} = D_{\text{arm}}$ (red symbols, bottom x axis) and core diameter D_{core} (for $D_{\text{arm}} = 2.1$ nm, blue symbols, upper x axis) for $L = 3.5$ nm. The solid lines are a guide to the eye. The dotted lines in the inset mark the position of CBM and VBM for $D = 2.1$ nm as a function of L from the mainframe, for a direct comparison of the dependences from the different geometrical parameters. This comparison highlights that the band edges position is most sensitive to the arm diameter D_{arm}, followed by core diameter D_{core} and is nearly independent on the arm length L.

The variation of the band edges with L (for a fixed $D = 2.1$ nm), D_{arm} (assuming the same core diameter and $L = 3.5$ nm), and D_{core} (for a fixed arm diameter of 2.1 nm and length of 3.5 nm) is presented in Fig. 1. We find that both CBM and VBM positions are nearly unchanged (they shift, respectively, by 10 meV and 26 meV), for an almost one order of magnitude increase in L, from 1.75 nm to 14 nm (Fig. 1, mainframe), whereas they shift by hundreds of meV (305 meV and 144 meV, respectively), for a much smaller increase (from $\sim$ 2 nm to 3.5 nm) in the TP's arm diameter D (Fig. 1 inset, red symbols).

A similar dependence on D and L was observed in elongated NCs (i.e., quantum rods, QRs), where electronic structure and optical properties were found to be dictated primarily by the arm's diameter.[35] Unlike in QRs, however, here this property derives from the peculiar localisation of the band edges' wave function occurring in TPs made of one material: due to the band alignment at the interface between zinc-blende core and wurtzite arms,[24,36] the CBM is localised in the TP's core[37] (whose size depends on D but not on L).

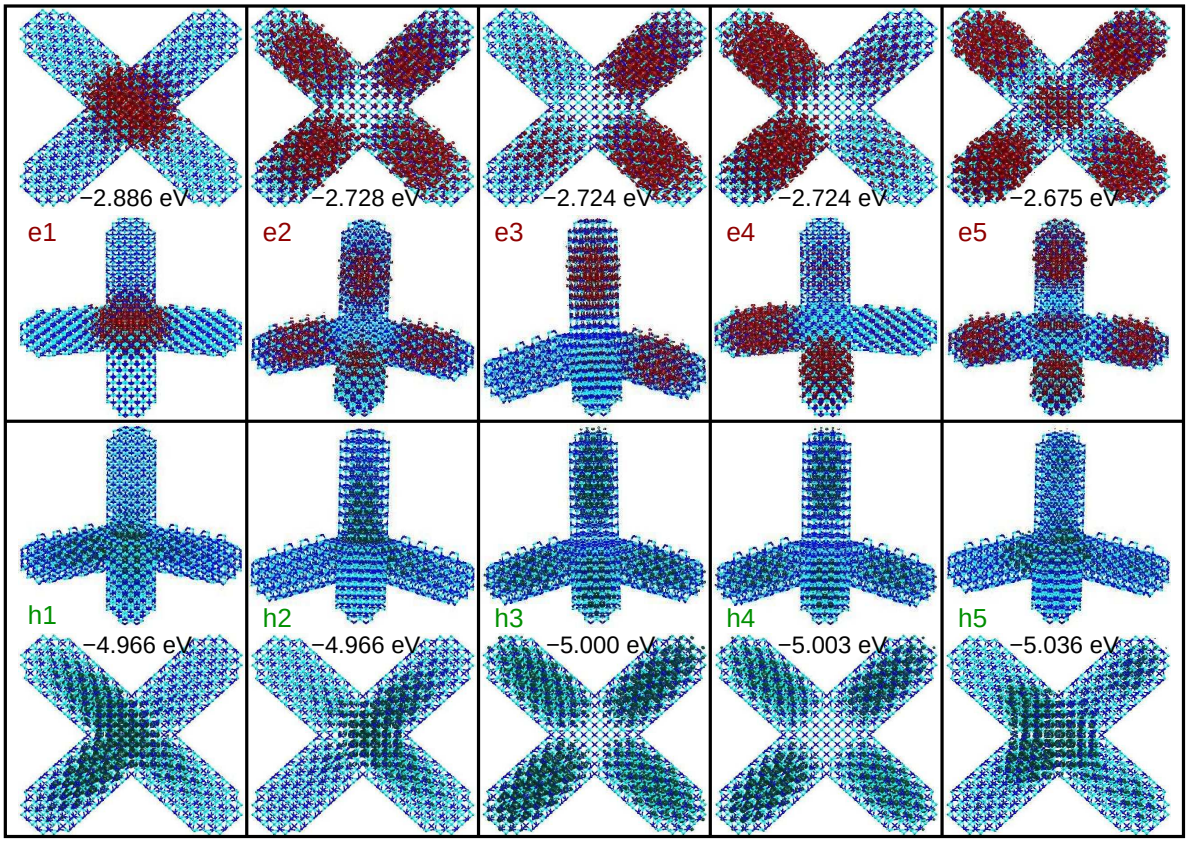

Figure 2: Charge densities for the uppermost 5 valence (green, bottom panels) and lowermost 5 conduction (red, top panels) band states, calculated for CdTe TPs with $D = 2.1$ nm and $L = 3.5$ nm (two different views of the TP are presented). Also reported are the corresponding energies, relative to vacuum. Blue and cyan dots represent Cd and Te atoms.

This is clearly shown in Fig. 2 and Fig. 3, where we present the calculated electron density distribution for conduction and valence states in TPs with $D = 2.1$ nm and, respectively, $L = 3.5$ nm and $L = 14$ nm. We see that in both nanostructures the CBM (e_1) is highly localised in the core, whereas the doubly degenerate VBM ($h_{1,2}$) also extends to

the arms, as was found to be the case in CdSe TPs.[37] Deeper VB states' wave functions present, alternately, a node (i.e., zero amplitude) or a peak in the core region. The excited CB states' wave functions exhibit the same behaviour in short-armed TPs (Fig. 2), but not in long-armed TPs (Fig. 3), where they always have a node in the core. Their symmetry is σ-like, as in a QR,[38] with zero (e_2-e_5), one (e_6-e_9), two (e_{10}), . . ., n nodes along each arm.

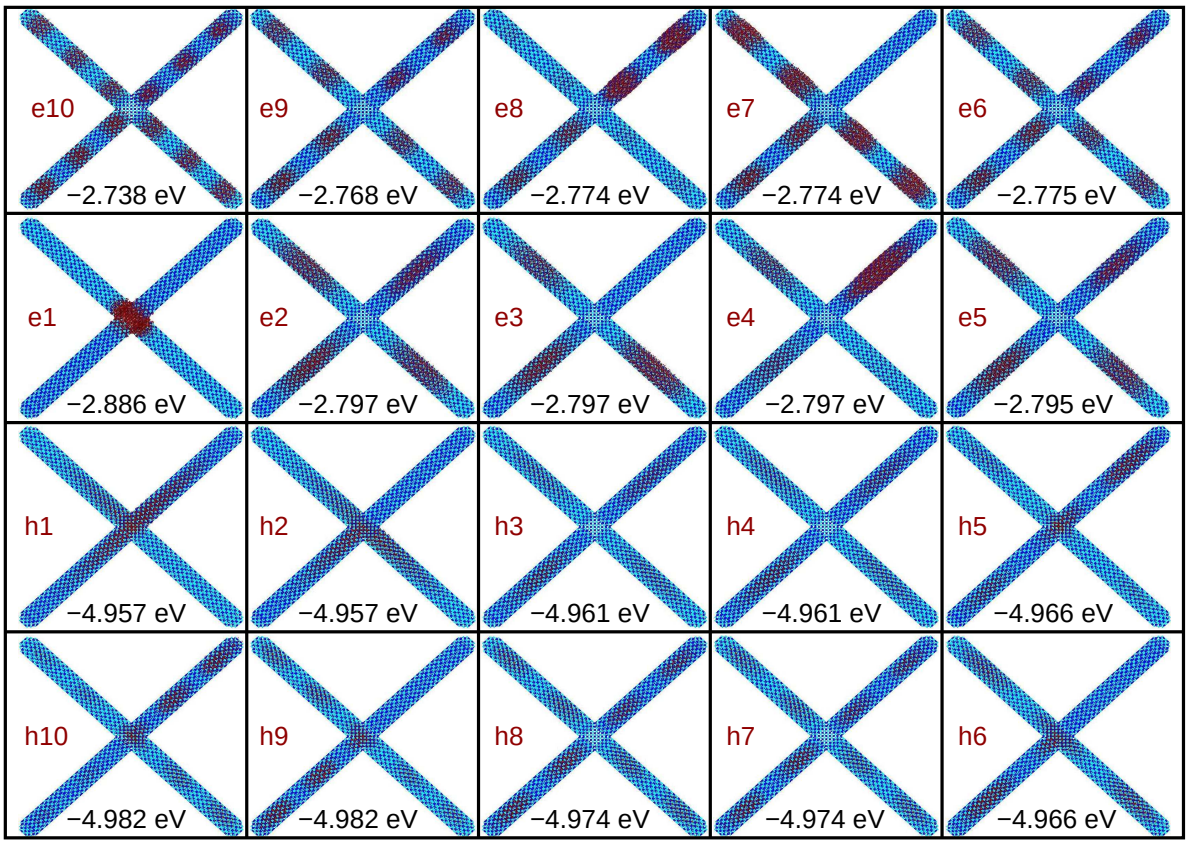

Figure 3: Charge densities (red) for the uppermost 10 valence (bottom 2 panels) and lowermost 10 conduction (top 2 panels) band states, with $D = 2.1$ nm and $L = 14$ nm. Also reported are the corresponding energies, relative to vacuum. Blue and cyan dots represent Cd and Te atoms.

As a consequence, the band edges position, hence the TP's band gap, is most sensitive to the arm diameter D_{arm} (Fig. 1 inset, red symbols), and the core diameter D_{core} (Fig. 1 inset, blue symbols), and is nearly independent of the arm length L (Fig. 1 mainframe), in agreement with experimental observation.[28]

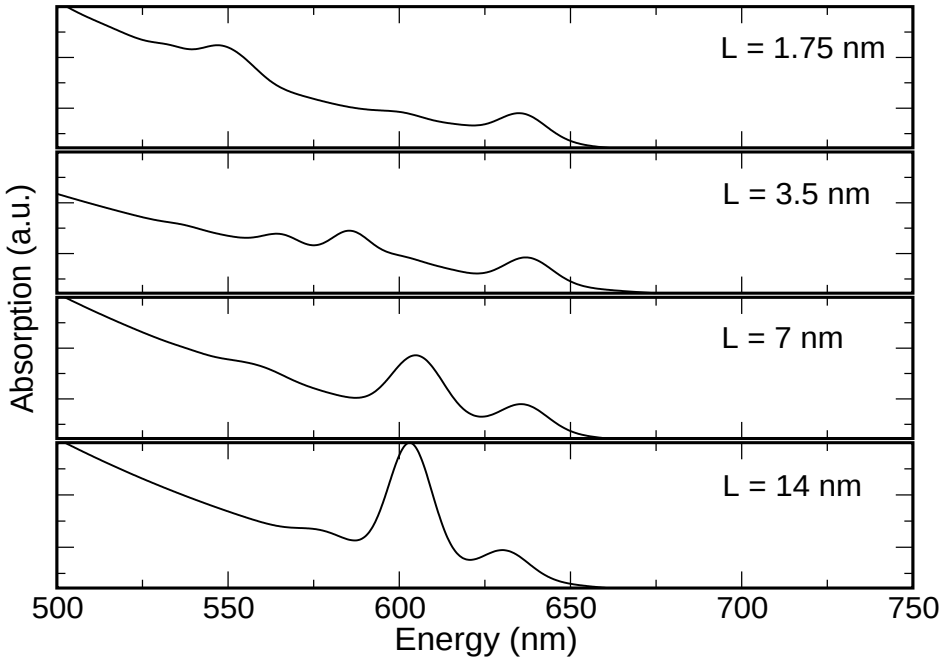

Figure 4: Absorption spectra calculated for TPs with $D = 2.1$ nm and different values of the arm length L.

The latter property is reflected in the optical absorption spectra calculated for TPs with $D = 2.1$ nm and 1.75 nm $\leq L \leq$ 14 nm (Fig.4), where the position of the absorption edge, corresponding to the transition between the band edges, is independent of the arm length, as observed experimentally.[24,36]

Similarly, we find that the radiative lifetime is also independent of L, as shown in Fig. 5 (mainframe), but sensitive to D (Fig. 5 inset), where it increases by a factor of 4 for an increase in diameter from about 2 nm to 3.5 nm. In summary, our results show that the electronic structure and optical properties *associated to the band edges* are insensitive to the TP's arm length, for a wide range of aspect ratios.

The question we want to address now is whether this insensitivity also applies to properties connected to excited states, and mechanisms relevant for light-emission applications, such as the electron intra-band relaxation or the biexciton recombination, which, in these systems, are mediated by Auger processes.

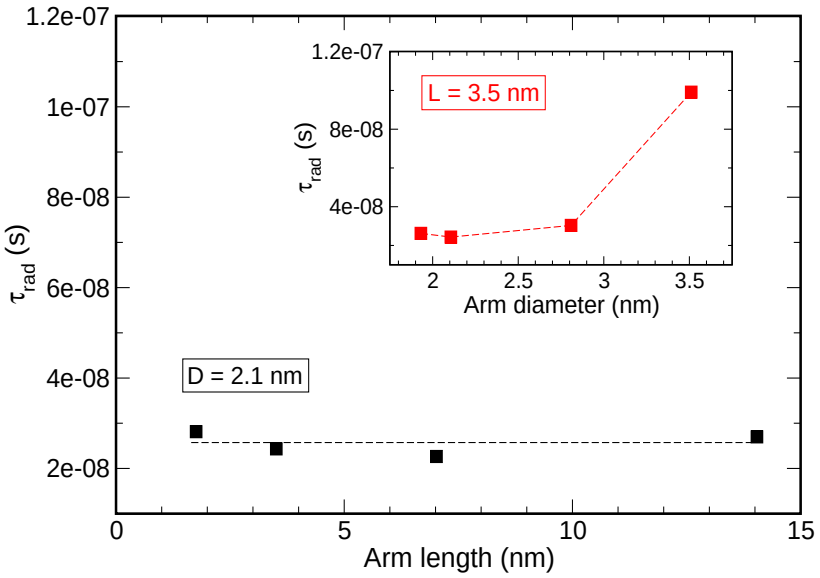

Figure 5: Radiative recombination lifetimes calculated, at room temperature, as a function of arm diameter (inset, red symbols) for $L = 3.5$ nm, and as a function of arm length (mainframe, black symbols) for $D = 2.1$ nm. The lines are a guide to the eye.

The AC lifetimes τ_{AC} calculated for TPs with $D = 2.1$ nm and $L = 3.5$, 7 and 14 nm are presented in Fig. 6, together with that of a spherical nanocrystal with a similar absorption edge ($R = 1.7$ nm) as a reference. The lifetime is shown here as a function of ΔE (the variation in the electron transition energy around the energy calculated for the ideal tetrapod - corresponding to $\Delta E = 0$), to account for possible energy dephasing effects due to ensemble effects (size distribution or shape anisotropy) and the influence of electric fields or charges in the environment. τ_{AC} increases by ~ 2 orders of magnitude for an increase in L of a factor of 4, from 3.5 to 14 nm, and by about 3 orders of magnitude with respect to a spherical NC. In contrast with the behaviour observed in spherical NCs, where τ_{AC} was found to depend linearly on the NC radius,[39] we find that, in TPs, the best fit to a power law yields a cubic dependence on L ($\tau_{AC} = A_0 L^3$, with $A_0 = 3.4 \times 10^{-3}$, black dashed line in Fig. S1a, Supporting Information), whereas the best overall fit yields $\tau_{AC} = B_0 \exp(0.4L)$ ($B_0 = 4.6 \times 10^{-2}$, green dashed line in Fig. S1a, Supporting Information). Similar dependences are also found on the volume (expressed as the total number of atoms, N_a),[40] i.e., $\tau_{AC} = C_0 N_a^{3.3}$ and $\tau_{AC} = D_0 \exp(N_a/1000)$ (with $C_0 =$

1.8×10^{-12} and $D_0 = 2.7 \times 10^{-2}$, black and green dashed lines in Fig. S1b, Supporting Information), showing that, despite following a L^3 scaling, τ_{AC} does not depend linearly on the TP volume.

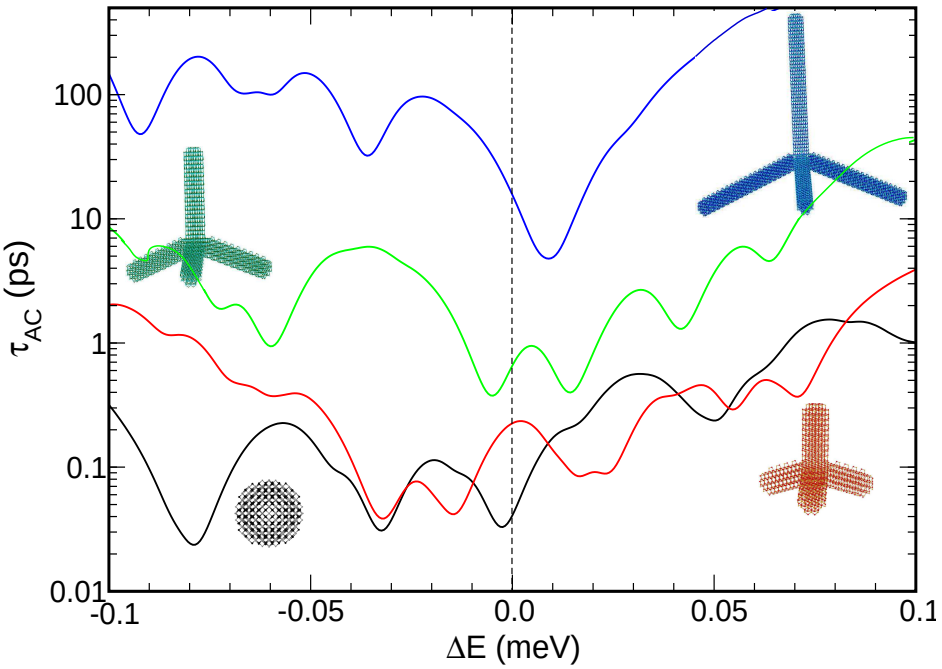

Figure 6: AC relaxation times in TPs with $D = 2.1$ nm and L=3.5 (red curve), 7 nm (green curve), and 14 nm (blue curve), as a function of ΔE (see main text). The black curve indicates the AC relaxation time calculated for a CdTe quantum dot with $R = 1.7$ nm for reference.

An approximately linear dependence on the volume has been observed for the AR lifetimes in spherical NCs made of CdSe,[41,42] PbSe,[43] Ge,[44] HgTe,[45] InAs,[44] and $FAPbBr_3$.[46,47] Interestingly, however, CdTe NCs have been reported to follow a V^{α} scaling[48] with $\alpha =$ 1.5 - 2.3, depending on the surface capping. For our calculated AR lifetimes, shown in Fig. 7, we find $\tau_{AR} = C_1 N_a^{1.6}$ (with $C_1 = 3.2 \times 10^{-4}$) to provide the best fit (see blue dashed line Fig. S2, Supporting Information), in agreement with the dependence on volume observed in spherical CdTe NCs. Furthermore the AR lifetime we calculate for a CdTe NC with $D = 3.4$ nm (red square in Fig. 7 and Fig. S2, Supporting Information) is in excellent agreement with the values experimentally measured for NCs with similar sizes[48] (magenta circle in Fig. S4, Supporting Information). In terms of dependence on L, we find

a nearly one order of magnitude increase in the AR lifetimes, when L increases from 3.5 nm to 14 nm (while, at the same time, both band gap - Fig. 4 - and radiative lifetime - Fig. 5 - remain constant), for an overall $\tau_{AR} \propto L^{1.5}$ scaling (black dashed line in Fig. 7). As it was the case for τ_{AC}, we find that an exponential function ($\tau_{AR} = B_1 \exp(0.2L)$ with $B_1 = 28.3$, green dashed line in Fig. 7) fits the data well too.

These results clearly show a complete decoupling between band edge optical properties, that determine band gap radiative lifetimes and PL quantum yields, and excited-state relaxation mechanisms that characterise the efficiency of the Auger processes. The origin of this separation lies in the spatial localisation of the electronic states involved in the two groups of transitions: as discussed above, CBM and VBM are localised primarily in the TP's core[37] (whose size is independent of L), whereas the excited states are mostly localised in the TP's arms, with a charge density that decreases with increasing arm length. This guarantees that the wave function overlap is large between the band edges, for any value of L, but becomes increasingly weak between band edge states and excited states, when L increases. A link between AR suppression and a reduction in the effective carrier density, which is inversely proportional to the NC volume, was indeed suggested by Htoon *et al.*,[50] to explain the increase in AR lifetimes they observed in QRs, compared to spherical NCs.

Our results are instead at odds with the hypothesis that slow AR is connected with decreased electron confinement,[49] as, despite exhibiting a nearly constant CBM energy (indication of a similar degree of electron confinement, which, as observed experimentally and discussed above, is determined by the arm diameter), TPs with same D and increasing L display increased AR lifetimes.

So far we have considered perfectly symmetric structures, where all four arms are equal in diameter and length. Before we conclude, we would like to briefly discuss the effect on our results of the presence of the following structural modifications, that may realistically occur in experimental samples: (i) asymmetry in arm length L or diameter D,

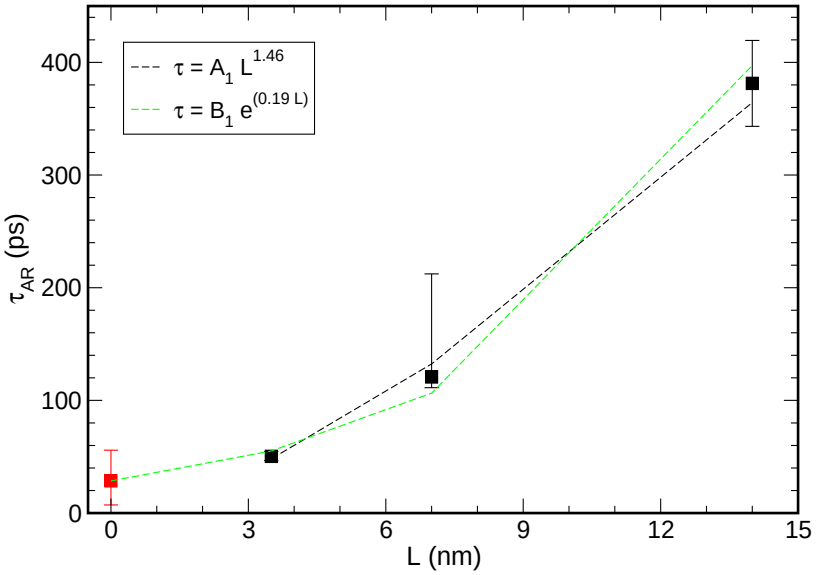

Figure 7: Auger recombination lifetimes calculated, as a function of arm length, for TPs with $D = 2.1$ nm (black symbols). The red symbol represents the AR lifetime calculated for a CdTe quantum dot with $R = 1.7$ nm for reference.

(ii) arm tapering, and (iii) crystal disorder. (i) Experimentally synthesized CdTe tetrapods have been reported[24] to have four arms that are equal to within a few percent. According to our calculations, a variation in D or L of up to 10% in one of the arms would not affect appreciably any of the decay times presented here, nor our conclusions. (ii) Substantial tapering is observed in TPs with CdSe arms,[33] but not in CdTe TPs.[24] According to atomistic SEPM calculations by Li and Wang,[37] in case of asymmetric elongated shapes, where one end is wider than the other, (the situation found in TP arm tapering), the hole wave function would avoid the narrow region of the structure, as would that of the CBM, but not those of higher energy electronic states, which would, however, still retain some localisation in the wider region of the structure. Arm tapering would, therefore, not affect band edge recombination, but may lead to a partial reduction of AC rates in short armed TPs, due to the reduced wave function overlap between initial and final states. The extent of such a reduction, however, should decrease with increasing arm length L, as the electron wave function moves away from the core (see 3), leaving our conclusions largely unaffected. (iii) More problematic, from the point of view of its impact on our results,

could be the possible presence, in experimental samples of tetrapods with CdTe arms, of structural disorder caused by the co-existence of both sphalerite and wurtzite domains.[33] Due to the different position of the band edges in zinc-blende and wurtzite, the presence of such mixed phases would create local shallow potential wells that could trap the electron. This would not affect band gap radiative recombination (as both states involved reside in the TP core). Similarly, the presence of such defects should not affect AR rates either, as the states involved in this process are either CBM and VBM (localised in the TP core) or highly excited states, whose energy (about E_g above/below CBM/VBM) is much larger than the band edges' discontinuity.

We have presented a comprehensive theoretical characterisation of colloidal CdTe TPs with arm diameters D ranging from 1.9 nm to 2.8 nm, and arm lengths L from 1.75 nm to 14 nm, containing from about 1000 to over 6000 atoms. We have investigated the dependence on both these parameters of the electronic structure, the optical spectra and the radiative recombination times. We found these nanostructures to have diameter-dependent and L-independent band edge energies, absorption onset and radiative lifetime. In contrast, Auger processes exhibit a marked dependence on the TP's arm length, as a consequence of the different spatial localisation of the excited states' wave functions compared to the band edges charge densities. This provides the ability to tune the TP's emission in the visible region of the electromagnetic spectrum, by selecting the appropriate arm diameter, while suppressing, at the same time, Auger cooling and recombination, by choosing a suitable value for the arms' length. In other words, these extremely versatile nanostructures enable, by virtue of their shape alone, a complete decoupling of Auger and radiative recombination. Furthermore, owing to their large volume, these systems also have the added benefits of an increased absorption cross section (directly dependent on the volume V), decreased thresholds for optical gain and for development of amplified spontaneous emission (both inversely dependent on V),[50] and reduced photoinduced absorption (also inversely dependent on V).[51] All these features make CdTe TPs ideally

suited for applications as efficient light-emitting media.

Theoretical Method

The TPs modelled in this work have a bulk-like crystal structure composed of a central zinc blende tetrahedral core with four (111)-equivalent facets, from which four wurtzite rod-like arms protrude.[24] As the zinc blende and the wurtzite lattices match along these directions, there is no discontinuity in the crystal structure at the interface. We recreate ideal conditions for a simulated seeded growth at each core/arm interface by checking the composition of the atomic layer at the core surface and proceeding with the correct layer stacking in the arm. This prevents the formation of stacking faults or other interfacial defects in our structures. We consider perfectly symmetric structures where all four arms have equal diameters D and lengths L. This condition is indeed realised in experimentally synthesized CdTe TPs, where the four arms are equal to within a few percent.[24] The unsaturated bonds at the TP surface are passivated by pseudo-hydrogenic, short-range potentials with Gaussian form.[52] This procedure ensures an ideal passivation, allowing us to focus on the intrinsic properties of these nanostructures. The single-particle energies and wave functions are obtained by solving the Schrödinger equation using the plane-wave semiempirical pseudopotential method described in Ref. [30], including spin-orbit coupling, and excitonic effects are accounted for via a configuration interaction scheme.[53]

Auger cooling and recombination times are calculated according to the procedure used previously in CdTe/CdSe TPs,[34] where a size- and position-dependent dielectric constant $\epsilon_{in} = \epsilon(R)$,[53] was assumed within the TP (and $\epsilon_{\text{out}} = 1$, was assumed for its environment), instead of the conventional regional screening with $\epsilon_{\text{in}} = \epsilon_{\text{bulk}}$ and $\epsilon_{\text{out}} = \epsilon_{\text{solvent}}$, developed in 22,54. We compared the results of the two approaches in a CdTe spherical nanocrystal with $R = 1.7$ nm and found that the calculated lifetimes agree for $\epsilon_{\text{out}} \approx 2.5 - 6$ (see Fig. S3 and Fig. S4, Supporting Information), which includes the

dielectric constants of the most commonly used solvents and capping groups.

Supporting Information Available

AC times as a function of arm length and TP volume; AR times as a function of TP volume; Auger Cooling and Recombination: comparison of the lifetimes calculated using two different approaches for the screening.

Acknowledgements

This work was undertaken on ARC3, part of the High Performance Computing facilities at the University of Leeds, UK. M.C. gratefully acknowledges financial support from the School of Electronic & Electrical Engineering, University of Leeds.

References

(1) Bruchez, M.; Moronne, M.; Gin, P.; Weiss, S.; Alivisatos, A.P. Semiconductor Nanocrystals as Fluorescent Biological Labels. *Science* **1998**, *281*, 2013-2016.

(2) Colvin, V. L.; Schlamp, M. C.; Alivisatos, A. P. Light-Emitting Diodes Made from Cadmium Selenide Nanocrystals and a Semiconducting Polymer. *Nature.* **1994**, *370*, 354-357.

(3) Klimov, V. I.; Mikhailovsky, A. A.; Xu, S.; Malko, A.; Hollingsworth, J. A.; Leatherdale, C. A.; Eisler, H. J.; Bawendi, M. G. Optical Gain and Stimulated Emission in Nanocrystal Quantum Dots. *Science* **2000**, *290*, 314-317.

(4) Talapin, D.V.; Lee, J.; Kovalenko, M. V.; Shevchenko, E. V. Prospects of Colloidal Nanocrystals for Electronic and Optoelectronic Applications. *Chem. Rev.* **2010**, *110*, 389-458.

(5) Kovalenko, M. V.; Manna, L.; Cabot, A.; Hens, Z.; Talapin, D.V.; Kagan, C. R.; Klimov, X. V. I.; Rogach, A. L.; Reiss, P.; Milliron, D. J.; Guyot-Sionnest, P.; Kostantatos, G.; Parak, W.J.; Hyeon, T.; Korgel, B.A.; Murray, C.B.; Heiss, W. Prospects of Nanoscience with Nanocrystals. *ACS Nano* **2015**, *9*,1012-1057.

(6) Kagan, C.R.; Lifshitz, E.; Sargent, E.H.; Talapin, D.V. Building Devices from Colloidal Quantum Dots. *Science*, **2016**, *353*, 885.

(7) Murray, C.B.; Norris, D.J.; Bawendi, M.G. Synthesis and Characterization of Nearly Monodisperse CdE (E = Sulfur, Selenium, Tellurium) Semiconductor Nanocrystallites. *J. Am. Chem. Soc.* **1993**, *115*, 8706-8715.

(8) Rogach, A. L.; Franzl, T.; Klar, T. A.; Feldmann, J.; Gaponik, N.; Lesnyak, V.; Shavel, A.; Eychmüller, A.; Rakovich, Y. P.; Donegan, J. F. Aqueous Synthesis of Thiol-Capped CdTe Nanocrystals: State-of-the-Art. *J. Phys. Chem. C* **2007**, *111*, 14628-14637.

(9) Greytak, A.B.; Allen, P.M.; Liu, W.; Zhao, J.; Young, E.R.; Popović Z.; Walker, B.J.; Nocera, D.G.; Bawendi, M.G. Alternating Layer Addition Approach to CdSe/CdS Core/Shell Quantum Dots With Near-Unity Quantum Yield and High On-Time Fractions. *Chem. Sci.* **2012**, *3*, 2028-2034.

(10) Chepic, D.I.; Efros, Al.L.; Ekimov, A.I.; Ivanov, M.G.; Kharchenko, V.A.; Kudriavtsev, I.A.; Yazeva T.V. Auger Ionization of Semiconductor Quantum Drops in a Glass Matrix. *J. Lumin.* **1990**, *47*, 113-127.

(11) Nirmal, M.; Dabbousi, B.O.; Bawendi, M.G.; Macklin, J.J.; Trautman, J.K.; Harris, T.D.; Brus, L.E. Fluorescence Intermittency in Single Cadmium Selenide Nanocrystals. *Nature* **1996**, *383*, 802-804.

(12) Vurgaftman, I.; Singh, J. Effect of Spectral Broadening and Electron-Hole Scattering on Carrier Relaxation in GaAs Quantum Dots. *Appl. Phys. Lett.*, **1994**, *64*, 232-234.

(13) Deng, Z.; Jeong, K. S.; Guyot-Sionnest, P. Colloidal Quantum dots Intraband Photodetectors. *ACS Nano*, **2014**, *8*, 11707-11714.

(14) Tisdale, W. A.; Williams, K.J.; Timp, B.A.; Norris, D.J.; Aydil, E.S.; Zhu, X.-Y. Hot-Electron Transfer from Semiconductor Nanocrystals. *Science*, **2010**, *328*, 15431547.

(15) Htoon, H.; Hollingsworth, J. A.; Dickerson, R.; Klimov, V. I.; Effect of Zero- to One-Dimensional Transformation on Multiparticle Auger Recombination in Semiconductor Quantum Rods. *Phys. Rev. Lett* **2003**, *91*, 227401.

(16) Zavelani-Rossi, M.;Lupo, M. G.; Tassone, F.; Manna, L.; Lanzani, G.; Suppression of Biexciton Auger Recombination in CdSe/CdS Dot/Rods: Role of the Electronic Structure in the Carrier Dynamics. *Nano Lett* **2010**, *10*, 3142-3150.

(17) Spinicelli, P.; Buil S.; Quelin, X.; Mahler, B.; Dubertret, B.; Hermier, J. P. Bright and Grey States in CdSe-CdS Nanocrystals Exhibiting Strongly Reduced Blinking. *Phys. Rev. Lett.* **2009**, *102*, 136801.

(18) Vela, J.; Htoon H.; Chen, Y.; Park, Y. S; Ghosh, Y.; Goodwin, F. M.; Werner, J. H; Wells, N. P.; Casson, J. L.; Hollingsworth, J. A. Effect of Shell Thickness and Composition on Blinking Suppression and the Blinking Mechanism in 'Giant' CdSe/CdS Nanocrystal Quantum Dots. *J. Biophotonics*, **2010** *3*, 706-717.

(19) Oron, D.; Kazes, M.; Banin, U. Multiexcitons in Type-II Colloidal Semiconductor Quantum Dots. *Phys. Rev. B* **2007**, *75*, 035330.

(20) Philbin, J. P.; Rabani, E. Auger Recombination Lifetime Scaling for Type I and Quasi-Type II Core/Shell Quantum Dots. *J. Phys. Chem. Lett.* **2020**, *11*, 5132-5138.

(21) Chen, Y.; Vela, J.; Htoon, H.; Casson, J. L.; Werder, D. J.; Bussian, D. A.; Klimov, V. I.; Hollingsworth, J. A. Giant Multishell CdSe Nanocrystal Quantum Dots with Suppressed Blinking. *J. Am. Chem. Soc*, **2008** *130*, 5026-5027.

(22) Califano, M. Suppression of Auger Recombination in Nanocrystals via Ligand-Assisted Wave Function Engineering in Reciprocal Space. *J. Phys. Chem. Lett.* **2018** *9*, 2098-2104.

(23) Müller, J.; Lupton, J.M.; Lagoudakis, P.G.; Schindler, F.; Koeppe, R.; Rogach, A.L.; Feldmann, J.; Talapin, D.V.; Weller, H. Wave Function Engineering in Elongated Semiconductor Nanocrystals with Heterogeneous Carrier Confinement. *Nano Lett.* **2005**, *5*, 2044-2049.

(24) Manna, L.; Milliron, D. J.; Meisel, A.; Scher, E. C.; Alivisators, A. P. Controlled Growth of Tetrapod-Branched Inorganic Nanocrystals. *Nat. Mater* **2003** *2*, 382-385

(25) Mishra, N.; Vasavi Dutt, V. G.; Arciniegas, M. P. Recent Progress on Metal Chalcogenide Semiconductor Tetrapod-Shaped Colloidal Nanocrystals and Their Applications in Optoelectronics. *Chem. Mater.* **2019** *31*, 9216-9242.

(26) Xie, R. G., Kolb, U., and Basché, T. Design and Synthesis of Colloidal Nanocrystal Heterostructures with Tetrapod Morphology. *Small* **2006**, *2*, 1454-1457.

(27) Malkmus, S.; Kudera, S.; Manna, L.; Parak, W.J.; Braun, M. Electron-Hole Dynamics in CdTe Tetrapods. *J. Phys. Chem. B* **2006**, *110*, 17334-17338.

(28) Tari, D.; De Giorgi, M.; Della Sala, F.; Carbone, L.; Krahne, R.; Manna, L.; Cingolani, R.; Kudera, S.; Parak, W. J. Optical Properties of Tetrapod-Shaped CdTe Nanocrystals. *Appl. Phys. Lett.* **2005**, *87*, 224101.

(29) Fang, L.; Park, J.Y. Mechanical and Electrical Properties of CdTe Tetrapods Studied by Atomic Force Microscopy. *J. Chem. Phys.* **2007**, *127*, 184704.

(30) Wang, L.-W.; Zunger, A. Local-Density-Derived Semiempirical Pseudopotentials. *Phys. Rev. B* **1995**, *51*, 17 398.

(31) Carbone, L.; Nobile, C.; De Giorgi, M.; Della Sala, F.; Morello, G.; Pompa, P.; Hytch, M.; Snoeck, E.; Fiore, A.; Franchini, I.R.; Nadasan, M.; Silvestre, A.F.; Chiodo, L.; Kudera, S.; Cingolani, R.; Krahne, R.; Manna, L. Synthesis and Micrometer-Scale Assembly of Colloidal CdSe/CdS Nanorods Prepared by a Seeded Growth Approach *Nano Lett.* **2007**, *7*, 2942-2950.

(32) Talapin, D. V., Nelson, J. H., Shevchenko, E. V., Aloni, S., Sadtler, B., and Alivisatos, A. P. Seeded Growth of Highly Luminescent CdSe/CdS Nanoheterostructures with Rod and Tetrapod Morphologies. *Nano Lett.* **2007** *7*, 2951-2959.

(33) Fiore, A.; Mastria, R.; Lupo, M. G.; Lanzani, G.; Giannini, C.; Carlino, E.; Morello, G.; De Giorgi, M.; Li, Y.; Cingolani, R.; Manna, L. Tetrapod-Shaped Colloidal Nanocrystals of II-VI Semiconductors Prepared by Seeded Growth. *J. Am. Chem. Soc.* **2009**, *131*, 2274-2282.

(34) Califano, M.; Zhou, Y. Inverse-Designed Semiconductor Nanocatalysts for Targeted CO_2 Reduction in Water. *Nanoscale* **2021**, *13*, 10024-10034.

(35) Katz, D.; Wizansky, T.; Millo, O.; Rothenberg, E.; Mokari, T.; Banin, U. Size-Dependent Tunneling and Optical Spectroscopy of CdSe Quantum Rods. *Phys. Rev. Lett.* **2002**, *89*, 086801.

(36) Manna, L.; Scher, E.C.; Alivisatos, A.P. Synthesis of Soluble and Processable Rod-, Arrow-, Teardrop-, and Tetrapod-Shaped CdSe Nanocrystals. *J. Am. Chem. Soc.* **2000**, *122*, 12700-12706.

(37) Li, J.; Wang, L.-W., Shape Effects on Electronic States of Nanocrystals. *Nano Lett.* **2003**, *3*, 1357-1363.

(38) Hu, J.; Wang, L.-W.; Li, L.-s.; Yang, W.; Alivisatos, A. P. Semiempirical Pseudopotential Calculation of Electronic States of CdSe Quantum Rods. *J. Phys. Chem. B* **2002**, *106*, 2447-2452.

(39) Klimov, V. I. Optical Nonlinearities and Ultrafast Carrier Dynamics in Semiconductor Nanocrystals. *J. Phys. Chem. B* **2000**, *104*, 6112-6123.

(40) We employ atom numbers to unequivocally express the volume, as opposed to using conventional units of nm^3, as volume estimates that use the latter are based on an assumed perfect geometrical (i.e., usually cylindrical) shape for the arms, that is never realised at the atomistic level.

(41) Klimov, V. I.; Mikhailovsky, A. A.; McBranch, D. W.; Leatherdale, C. A.; Bawendi, M. G. Quantization of Multiparticle Auger Rates in Semiconductor Quantum Dots. *Science* (Washington, DC, U. S.) **2000**, *287*, 1011-1013.

(42) Pandey, A.; Guyot-Sionnest, P. Multicarrier Recombination in Colloidal Quantum Dots. *J. Phys. Chem. Lett*, **2007**, *127*, 111104.

(43) Klimov, V. I.; McGuire, J. A.; Schaller, R. D.; Rupasov, V. I. Scaling of Multiexciton Lifetimes in Semiconductor Nanocrystals. *Phys. Rev. B* **2008**, *77*, 195324.

(44) Robel, I.; Gresback, R.; Kortshagen, U.; Schaller, R. D.; Klimov, V. I. Universal Size-Dependent Trend in Auger Recombination in Direct-Gap and Indirect-Gap Semiconductor Nanocrystals. *Phys. Rev. Lett* **2009**, *102*, 177404.

(45) Melnychuk, C.; Guyot-Sionnest, P. Slow Auger Relaxation in HgTe Colloidal Quantum Dots. *J. Phys. Chem. Lett.* **2018**, *9*, 2208-2211.

(46) Castañeda, J. A.; Nagamine, G.; Yassitepe, E.; Bonato, L. G.; Voznyy, O.; Hoogland, S.; Nogueira, A. F.; Sargent, E. H.; Cruz, C. H. B.; Padilha, L. A. Efficient Biexciton Interaction in Perovskite Quantum Dots Under Weak and Strong Confinement. *ACS Nano* **2016**, *10*, 8603-8609.

(47) Li, Y.; Ding, T.; Luo, X.; Tian, Y.; Lu, X.; Wu, K. Synthesis and Spectroscopy of

Monodispersed, Quantum-Confined $FAPbBr_3$ Perovskite Nanocrystals. *Chem. Mater.* **2020**, *32*, 549-556.

(48) Kobayashi, Y.; Pan, L.; Tamai, N. Effects of Size and Capping Reagents on Biexciton Auger Recombination Dynamics of CdTe Quantum Dots. *J. Phys. Chem. C* **2009**, *113*, 11783-11789.

(49) Melnychuk, C.; Guyot-Sionnest, P. Multicarrier Dynamics in Quantum Dots. *Chem. Rev.* **2021**, *121*, 4, 2325-2372.

(50) Htoon, H.; Hollingsworth, Malko, A.V.; J. A.; Dickerson, R.; Klimov, V. I. Light Amplification in Semiconductor Nanocrystals: Quantum Rods Versus Quantum Dots. *Appl. Phys. Lett* **2003**, *82*, 4776-4778.

(51) Klimov, V.I. in *Semiconductor and Metal Nanocrystals: Synthesis, Electronic and Optical Properties*, edited by V. I. Klimov (Marcel Dekker, New York, 2003), Chapter 5.

(52) Graf, P.A.; Kim, K.; Jones, W.B.; Wang, L.W. Surface Passivation Optimization Using DIRECT. *J. Comp. Phys.* **2007**, *224*, 824-835.

(53) Franceschetti, A.; Fu, H.; Wang, L.-W.; Zunger, A. Many-body Pseudopotential Theory of Excitons in InP and CdSe Quantum Dots. *Phys. Rev. B* **1999**, *60*, 1819-1829.

(54) Wang, L.-W.; Califano, M.; Zunger, A.; Franceschetti, A. Pseudopotential Theory of Auger Processes in CdSe Quantum Dots. *Phys. Rev. Lett.* **2003**, *91*, 056404.